Nano World Journal

http://dx.doi.org/10.17756/nwj.2017-039

Research Article

Open Access

Surface Modification Efficiency of Titanium-based Particles with an Alkyl Phosphate

Igor Lopes Soares, Elton Jorge da Rocha Rodrigues, Taís Nascimento dos Santos, Emerson Oliveira da Silva and Maria Inês Bruno Tavares*

Instituto de MacromoléculasProfessora Eloisa Mano, Universidade Federal do Rio de Janeiro, Rio de Janeiro, Brazil

***Correspondence to:**
Maria Inês Bruno Tavares
Instituto de Macromoléculas Professora Eloisa Mano, Universidade Federal do Rio de Janeiro
Av. Horácio Macedo 2030, Bloco J
Centro de Tecnologia, Ilha do Fundão
Rio de Janeiro, CEP 21941-598, Brazil
Tel: +55 21 2562-8103
E-mail: mibt@ima.ufrj.br

Received: November 22, 2016
Accepted: January 31, 2017
Published: February 03, 2017

Citation: Soares IL, Rodrigues EJR, dos Santos TN, da Silva EO, Tavares MIB. 2017. Surface Modification Efficiency of Titanium-based Particles with an Alkyl Phosphate. *NanoWorld J* 3(1): 11-17.

Published by United Scientific Group

Abstract

This article reports the efficiency of surface modification of titanium particles based on an alkyl phosphate. Different techniques were used to evaluate the behavior of the samples after modification, in terms of better particle dispersion tendency in response to type and quantity of modifier incorporation (TiO_2 anatase in crystalline form). The TiO_2 nanotubes were synthesized and their surfaces were modified by chemical reaction. Concerning elucidation of the efficiency of anchoring the modifier on the surface of the nanoparticles, the proposed approaches were effective because the treated particles had more active sites. This resulted in efficient disaggregation of the particles, generating lower aggregation and likely smaller particles within the aggregates, by decreasing particle-particle interaction. The use of NMR relaxometry was very useful to probe the chemical modification and also to ascertain the extent of surface modification.

Keywords

Synthesis, Nanoparticles, TiO_2, TD-NMR, STEM, Tauc relation

Introduction

The incorporation of inorganic nanoparticles in polymers is a viable method to produce materials with desired properties and functions [1]. Among inorganic nanoparticles, titanium dioxide (TiO_2) is one of the most promising for development of new materials, because of its important features such as photocatalytic activity, antibacterial properties, UV resistance and antistatic behavior [2]. It is known that factors like surface treatment, particle size and crystal form affect the photocatalytic activity of TiO_2 particles. As regards photodegradation of polymers, TiO_2 in anatase form is usually more photoactive than in rutile form [3]. The particles' surface modification with phosphonic acids and their derivatives in the form of esters is attracting increasing interesting of researchers because these can be added to materials for many applications, such as ceramic membranes, photoelectrochemical cells based on nanocrystalline TiO_2 film and enzymatic catalysts. The anchoring of organo-phosphorus species on the surface of these TiO_2 particles exhibits good stability and can enhance the photocatalytic characteristic of this semiconductor [4]. Researchers have investigated the mechanism by which particles become photosensitive in order to manipulate the wettability, increase the surface area of these by UV light, enhance thermal and chemical stability as well as improve the biocompatibility of TiO_2 after surface area modifications with organic or inorganic materials [5].

This study first aimed to obtain nanoparticles with tubular morphology based on TiO_2 and also to organically modify the surface area of these nanoparticles with

alkyl phosphate to increase their physical-chemical affinity for hydrophobic molecules (of which most polymer materials are composed). The second objective was to characterize the new materials, mainly by nuclear magnetic resonance in the time domain (TD-NMR).

Experimental Details

Materials

TiO_2 anatase in crystalline form was supplied by Sigma-Aldrich (USA). The nanoparticles' size was approximately 25 nm, with 99.7% purity, and the density was 3.9 gcm^{-3}. Chloridric acid (P.A.), alkyl phosphate and anhydrous ethanol were obtained from Vetec (Brazil).

Methods

Two experimental stages were performed. The first one consisted of synthesizing TiO_2 nanoparticles [6], with high aspect ratio and tubular morphology. The samples obtained were called *Carga Aa* (particles obtained immediately after the chemical synthesis process) and *Carga Ac* (*Carga Aa* after calcination). They were characterized by UV, XRD, BET, SEM and STEM.

The second experimental stage consisted of surface modification by chemical reaction of the nanoparticles generated, as well as the commercial TiO_2 particles. The reaction products were characterized by TGA, TD-NMR and EDX.

Synthesis of the TiO_2 nanoparticles

In summary, a suspension of TiO_2 in an aqueous solution of NaOH 10 $mol.L^{-1}$ and KOH 10 $mol.L^{-1}$, under reflux (100 °C), with magnetic stirring was left to react during 48 h. After this period, the suspension was decanted. The solid material was washed several times until pH 7 ± 0.1. To convert the TiO_2 nanoparticles to protonated form, an aqueous acid solution was added containing HCl 0.1 $mol.L^{-1}$ until attaining H = 2 ± 0.1. The mixture was allowed to stand during 30 minutes, and then was filtered and washed with deionized water until reaching pH 5 ± 0.1. Last, the TiO_2 nanoparticles were dried in a forced-air oven at 120 °C [6]. The particles obtained were called *Carga Aa*. Some of these were calcinated in a muffle furnace at 500 °C for 2 h, called *Carga Ac*.

Particles' surface modification

To anchor the modifier to the active sites of the titanium particles prepared in the previous step, three approaches were tested:

Approach 1

A solution of 1.5 g of alkyl phosphate in 375 ml of ethanol and 125 ml of water was prepared in a 1000 ml Erlenmeyer flask under stirring. In parallel, 1 g of a suspension of commercial TiO_2 was prepared in 100 ml of acidified water. The suspension containing the nanoparticles was added dropwise to the solution containing the modifier. After TiO_2 addition, the system was left under stirring at room temperature during 48 h. The product was named TiO_2 I.

Approach 2

A solution of 1.5 g of alkyl phosphate in 250 ml of ethanol was prepared in a 500 ml Erlenmeyer flask, under stirring. In parallel, a suspension of 1 g of commercial TiO_2 in 100 ml of acidified ethanol was prepared. The suspension containing the nanoparticles was added dropwise to the solution containing the modifier. Then the system was left under stirring at room temperature during 48 h. The product was named TiO_2 II.

Approach 3

A solution of 1.5 g of alkyl phosphate in 250 ml of ethanol and 84 ml of water was prepared in a 500 ml Erlenmeyer flask, under stirring. In parallel, a suspension of 1 g of commercial TiO_2 in 100 ml of acidified ethanol was prepared. The solution containing the modifier was added dropwise to the nanoparticle solution. Then the system was left under stirring at room temperature during 48 h. The product was named TiO_2 III.

Approach 3 was also applied to the synthesized nanoparticles after being calcinated (*Carga Ac*).

The products of the synthesis and the surface modifications were washed by filtration with ethanol and acetone to remove the non-reactive molecules. Then they were dried in a forced-air oven at 120 °C for 10 minutes and kept in a desiccator.

Characterization

X-ray diffraction (XRD)

All samples were analyzed by XRD using a Rigaku D/Max 2400 diffractometer, with nickel-filtered CuKα radiation of wavelength 1.54 Å, at room temperature. The 2θ scanning range was varied from 2° to 90°, with 0.05° steps, operated at 40 KV and 30 mA.

Time domain nuclear magnetic resonance (TD-NMR)

The 1H NMR relaxation measurements were performed with a Maran Ultra 23 low-field NMR spectrometer, operating at 23.4 MHz (for protons) and equipped with an 18 mm variable temperature probe operating at 300 K. Proton spin-lattice relaxation time (T1H) was measured using the inversion-recovery pulse sequence (D1- π - τ - π/2 - acquisition), with a recycle delay of 5T1 (e.g., D1 of 5 s), and π/2 pulse of 7.5 ms, calibrated automatically by the instrument's software. The amplitude of the FID was sampled for 40 τ data points, ranging from 0.1 to 5000 ms, with 4 scans each point. The data were obtained using the Winfit program with the aid of WinDXP software that comes with the equipment. The parameters employed in the acquisition are listed in Table 1.

Energy dispersive X-ray spectroscopy (EDX)

The analysis was performed in a vacuum, during 320 seconds, with a Shimadzu EDX-720 spectrometer.

Thermogravimetric analysis

The thermogravimetric analysis (TGA) was carried out in a TA Instruments Q500 apparatus (USA) from 27 °C to 700 °C

under nitrogen flow (50 mL/min) at a 10 °C /min heating rate.

Table 1: Parameters employed in the single pulse sequence.

Parameters	Values
Pulse sequence	90º-Acquisition
90º pulse- µs	7.0
Number of scans	128
Dwell time – µs	2.0
Size of acquisition buffer	1024
Recycle delay – s	1.0
Receptor gain - %	5
Probe dead time – µs	8.5
Receiver dead time – µs	4.0

The results were processed with the help of the Origin v. 8.5 software.

UV measurements

The UV-Vis absorption spectra and band gap energy of the samples were determined using a Shimadzu UV-2401 PC UV-Vis spectrophotometer (Japan). The optical absorption measurements were scanned over the range of 190-800 nm, using a 1 cm quartz cuvette. The performance was compared against a standard suspension containing 10 mg of sodium dodecyl sulfate (99% wt PA, ACS, Panreac), 20 ml of distilled water and 2 mg of *Carga Ac*. The system was left under ultrasound agitation for 30 min. The optical band gap E_g was calculated by curve extrapolation using a data processing platform (Fitteia Report v. 1.0), an internet-based fitting service [7].

Scanning electron microscopy (SEM) and scanning transmission electron microscopy (STEM)

The SEM and STEM images of the particles were obtained with an FEI Nova 200 dual beam SEM (University of Minho, Portugal) with ultra-high resolution field emission scanning, resolution of 1.0 nm, at 15 kV for SEM and 0.8 nm at 30 kV in transmission mode.

Surface area measurement (BET)

Nitrogen adsorption/desorption isotherms were obtained using a Micromeritics ASAP 2010 analyzer. The surface area, diameter and pore size distribution were determined by Brunauer-Emmett-Teller (BET) measurements.

Results and Discussion

XRD and BET surface area

Figure 1 presents the diffractograms of the nanoparticles synthesized with and without thermal treatment in comparison to commercial TiO_2. The diffraction pattern showed that the non-calcinated samples, *Carga Aa*, had the typical pattern of nanocrystalline materials, with the appearance of characteristic peaks at 2θ = 9.8º, 24º and 28º. The value of the peak around 9.8º (002) is attributed to the creation of interlayer spacing in the particles in the tubular form. Since the peak intensity

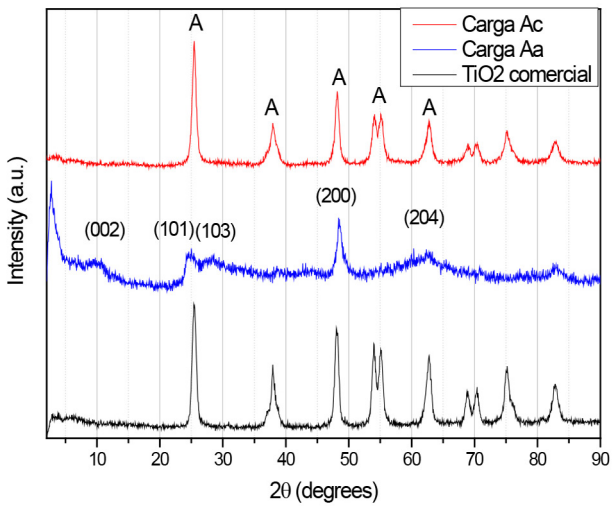

Figure 1: X-ray diffractograms of the commercial and synthesized filler in nanocrystalline form (*Carga Aa*) and after heat treatment (*Carga Ac*), in which (A) refers to anatase crystalline phase.

values at 2θ = 24º and 28º are attributed to the Na:H ratio, the slight variation of the value at 2θ = 24º suggests there was some exchange between sodium ions and protons during drying in acidic environment (pH=5), due to this change in the crystalline structure [6, 8-10]. However, these results indicate the need for calcination to order atoms in the crystal and obtain a higher crystallinity degree. The diffractograms of the calcined samples (*Carga Ac*) had better definition of the diffraction peaks after heat treatment at 500 °C, demonstrating an increase in crystallinity of the material, which remained in the crystalline anatase form.

Figure 2 contains the isotherms obtained by adsorption/desorption of N_2 for the materials obtained to get response on samples' pore and surface area. The results indicated porous characteristics for commercial TiO_2, which presented surface area of 54.5 m^2/g, pore volume of 0.26 cm^3/g and average pore diameter of 190.8 Å. For the loads synthesized in the laboratory, the values for *Carga Aa* were surface area of 179.1 m^2/g, pore volume of 0.30 cm^3/g and average pore diameter of 67.4 Å; while the *Carga Ac* presented surface area of 120.2 m^2/g, pore volume of 0.60 cm^3/g and average pore diameter of 200.8 Å. Observing the curves in Figure 2, it is possible infer that the materials were similar to isotherm type III, characteristic of multilayer absorption, which can occur in nonporous solids, macroporous solids or mesoporous materials. This happens because materials of the same chemical nature, although presenting different specific area values, will have similar isotherms. On the other hand, the knowledge of this property is of great importance because the greater surface area provides space for a larger number of active sites for reaction. The curves show hysteresis occurred in all samples, with commercial TiO_2 and *Carga Ac* being more characteristic of type H-1, according to the classification of the International Union of Pure and Applied Chemistry (IUPAC). This type is generally associated with materials composed of rigid agglomerated spherical particles of uniform size or cylindrical particles with open ends, in both cases having evenly spaced pores. However, the sample *Carga Aa* presented type H-3 behavior, generally

associated with non-rigid aggregates of particles with conical or pyramidal shape with slit pores of wide size variation. The results observed demonstrated that the modification by chemical treatment and calcination provides different families of nanoparticles [11-13].

UV-Vis spectra

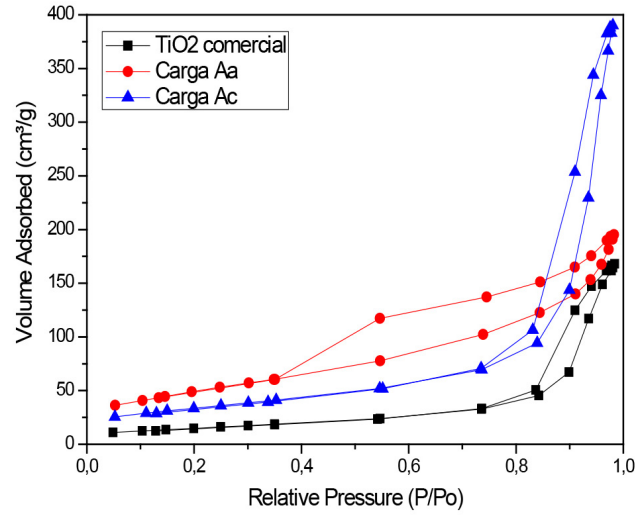

Figure 2: Isotherms of adsorption and desorption of N_2 of the commercial and synthesized filler in amorphous form (*Carga Aa*) and after heat treatment (*Carga Ac*).

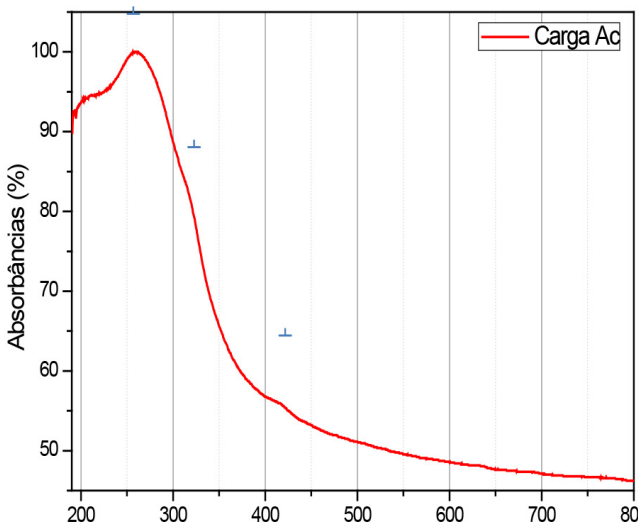

Figure 3: UV-visible absorption spectrum of synthesized filler after heat treatment (*Carga Ac*).

The absorption spectrum of *Carga Ac* is shown in Figure 3, demonstrating maximum absorption at 258.5 nm and two wider regions at higher wavelengths (range of 303.5 to 334.5 nm and 418 nm, respectively). Those absorption bands are associated with transitions of electrons from valence band to conduction band and they depend on the material's morphology. The increase in the maximum absorption of modified nanoparticles in relation to commercial TiO_2 indicates alteration of their structure. The optical gap was calculated utilizing Tauc's relation, according to Equations 1 and 2:

$$\alpha h_\upsilon = A\left(h_\upsilon - E_g\right)^{1/2} \quad \text{.....(1)}$$

$$\upsilon = C/\lambda \upsilon = C/\lambda \quad \text{.....(2)}$$

Where, hυ is the photon energy, α is the absorption coefficient, υ is the frequency, C is the speed of light and λ is the wavelength. The bandgap can be estimated through linear extrapolation of the curve (αhυ)2 vs. hυ, as shown in Figure 4. The absorption coefficient α can be calculated from the measured absorbance (A) using the following Equation 3:

$$\alpha = \frac{2.303\rho\ 10^3 A}{I_c M} \quad \text{.....(3)}$$

Where the density (ρ) is 3.9 gcm-3 (referring to commercial TiO_2), the molar mass (M) is 79.9 $gmol^{-1}$, c is the molar concentration of particles and the optical length (l) is 1 cm. The bandgap value estimated by the intercept of the tangent line with the X axis (hυ) was 3.15 eV for Carga Ac (Figure 4), with 3.52 eV being the typical gap value for TiO_2 in the anatase form, according to the literature. This bandgap value of the synthesized particles is similar to that described in the literature for particles with tubular form. This result also indicated more intense absorption of visible light [8, 14, 15].

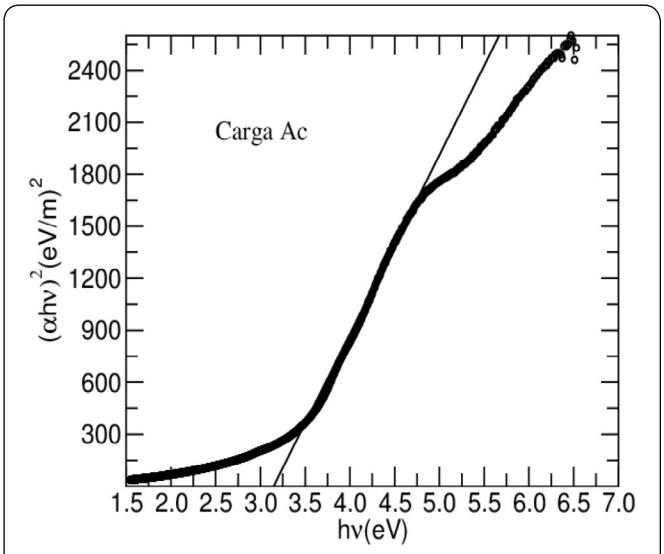

Figure 4: Plot of (*αhυ*)2versus photon energy (*hυ*) corresponding to Tauc's relation for estimating bandgap of synthesized filler after heat treatment (*Carga Ac*).

Modifications of TiO_2 particles

The approaches used for chemical modification of nanoparticles generated products with different macroscopic characteristics. Approach 1 produced a pasty and agglomerated material; Approach 2 produced loose particulate material, so less modifier quantity was incorporated than in the materials obtained by Approach 3, which is considered the standard

approach to obtain the materials studied. Anchoring the surface modifier probably occurred through the reaction between the acid sites; both Lewis and Brönsted are present in the TiO_2 particles and the alkyl phosphate group [16].

TD-NMR and EDX

TD-NMR was employed in this study for characterization of the materials after chemical modification, because it is a fast and nondestructive spectroscopic technique that does not require any previous treatment [17-19]. Since the signal intensity is proportional to the number of hydrogen nuclei present in the analyte, high NMR signal intensity (Amplitude Intensity, A.I.) is an indication of a greater amount of alkyl phosphate anchored on the nanoparticles' surface. This phenomenon is demonstrated in Figure 5. Analysis of TiO_2 in relation to surface modification reaction shows that the signal detected by the equipment was small, indicating primarily some water molecules physisorbed on the nanoparticles' surface. The signals from the chemically modified nanoparticles are more significant and are related to the aliphatic fraction of the modifier through observation of their ^1H nuclei.

Figure 6 shows a comparison between the maximum

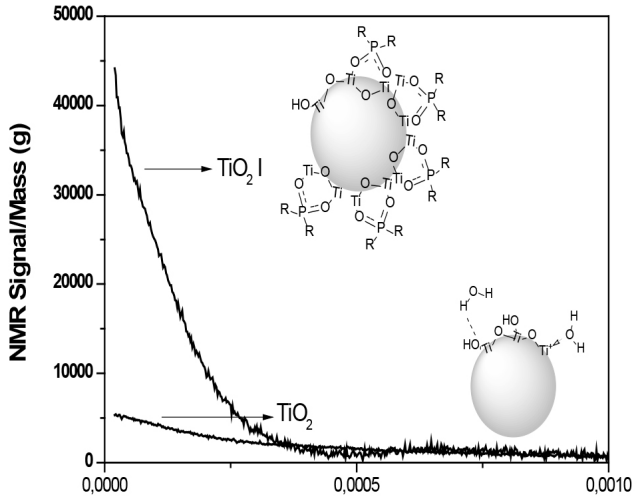

Figure 5: TD-NMR signal, divided by the mass of the sample, as a function of the quantity of hydrogen nuclei present in the analyte. As the surface of the TiO_2 nanoparticle is modified, the signal's intensity rises.

values of the signals obtained by NMR of the three modification approaches used, showing that TD -NMR is able to detect differences in the amounts of modifier anchored to the nanoparticles. It is thus a quick and convenient method to check the efficiency of the chemical modification of the synthesized systems [18, 19].

The EDX technique was also employed to observe the percentage of phosphorus present in the modified particles. The highest Pearson correlation ($r^2 = 0.999$) obtained by EDX corroborates those found by TD- NMR, employing Approach 1 (TiO_2 I). These results indicate higher percentage of P_2O_5, showing that it is the best system to anchor the phosphate groups in the active TiO_2 sites (Table 2). According to these excellent correlations between EDX and TD-NMR; we can say that this last method, proposed in this work, can be used in tandem with EDX analysis to confirm the presence and extent of anchoring organic surface modifiers in oxides, even when they have long carbon chains.

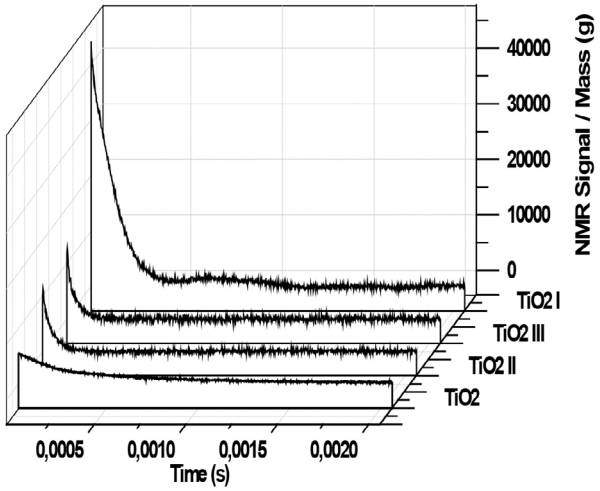

Figure 6: TD-NMR signals, divided by each sample's mass, showing the technique's sensitivity to modifier anchoring efficiency.

Table 2: Correlation between TD-NMR and EDX results.

Sample	TD-NMR (A.I.)	EDX (% of P_2O_5)
TiO_2 I	44176	3.4
TiO_2 II	10478	1.1
TiO_2 III	12836	1.3
Carga Ac MOD	28510	3.7

Thermogravimetric analysis

The thermal degradations of the nanoparticles were evaluated before and after chemical anchoring of the alkyl phosphate. The results obtained by TGA shown in Figure 7, referring to the commercial TiO_2 and *Carga Ac* without chemical modification; indicate that both have the standard behavior of inorganic systems, which generally have high thermal stability in the temperature range analyzed here. We only observed a single mass loss event, in a single step of approximately 1% for the synthesized nanoparticles in relation to the commercial TiO_2, in the range from 50 to 200 °C. That process can be associated with the loss of water adsorbed on the surface of the particles and the greater mass loss in the case of *Carga Ac* can be due to the greater number of active sites of the hydroxyl groups on the surface, possibly resulting in greater water adsorption capacity. This result indicates concordance with the higher specific areas and pore volumes described in the analysis of the surface area for the sample. To verify both the modification process and efficiently evaluate the thermal stability of the modifier, the particles were also evaluated after chemical modification. For comparison purposes, a commercial TiO_2 batch was anchored with alkyl phosphate employing the same method as for sample *Carga Ac* and was submitted to TGA. The results showed a single thermal degradation step of alkyl phosphate of around 7% by weight for the modified (TiO_2 MOD) and 17% mass for modified *Carga Ac* (*Carga Ac*

MOD), demonstrating the effect of the increased surface area, contributing to the formation of tubular particles synthesized in this work.

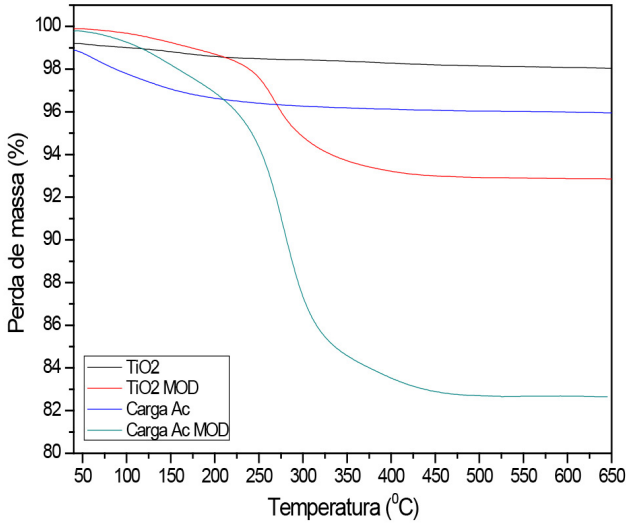

Figure 7: TGA curves of the initial and maximum degradation temperatures of the commercial TiO_2 and synthesized filler after heat treatment (*Carga Ac*), for unmodified and organically modified particles.

SEM and STEM analyses

Figure 8 shows the images obtained by scanning electron microscopy and scanning transmission electron microscopy of the commercial TiO_2 and synthesized materials, with or without surface modification, using Approach 3. Even at the highest magnification possible, the resolution of the micrographs was not sufficient to distinguish the nanoparticles' morphology. However, estimated calculations provided by the equipment showed that the particles had nanometric size and that the particles synthesized in the laboratory were smaller than commercial TiO_2. A tendency for smaller size of the nanoparticle aggregates can also be identified as the samples passed from a regime of anchoring using alkyl phosphate to extensive anchoring by the organo-modifier, which indicates that the surface modification was likely responsible for the decreased affinity between the particles.

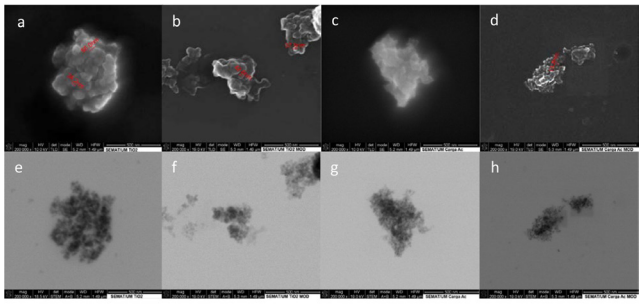

Figure 8: SEM and STEM images of the commercial and synthesized filler after heat treatment (*Carga Ac*), unmodified (***a,e*** *and* ***c,g***) and organically modified particles (***b,f*** *and* ***d,h***), respectively.

Conclusions

By comparing the different results, we can say that the synthesis of the nanoparticles was efficient. The final shape of the particles was different from conventional spherical form of oxides. Instead, they presented cylindrical shape with open ends, in line with the descriptions found in the literature for the synthesis of particles in tubular form, without losing predominance of the anatase crystalline form. The modification also reduced the bandgap value of the synthesized materials. This can indicate a possible increase in the catalytic efficiency of the synthesized particles. Concerning the elucidation of the anchoring efficiency of the modifier on the surface of the nanoparticles, it is evident that the proposed approaches were effective because the treated particles had more active sites. This resulted in efficient disaggregation of the particles, generating lower aggregation and likely smaller particles within the aggregates by decreasing particle-particle interaction. Finally, the results show that time domain nuclear magnetic resonance (TD-NMR) can be a quick and convenient method to check the chemical modification efficiency, being capable of detecting differences in the amounts of modifiers anchored to the nanoparticles.

References

1. Ruiterkamp GJ, Hempenius MA, Wormeester H, Vancso GJ. 2011. Surface functionalization of titanium dioxide nanoparticles with alkanephosphonic acids for transparent nanocomposites. *Journal of Nanoparticle Research* 13(7): 2779-2790. doi: 10.1007/s11051-010-0166-1
2. Wei Z, Wang G, Wang P, Liu L, Qi M. 2012. Crystallization behavior of Poly(e-caprolactone)/TiO_2 nanocomposites obtained by *in situ* polymerization. *Polymer Engineering and Science* 52(5): 1047-1057. doi: 10.1002/pen.22165
3. Liu Z, Jin J, Chen S, Zhang J. 2011. Effect of crystal form and particle size of titanium dioxide on the photodegradation behaviour of ethylene-vinyl acetate copolymer/low density polyethylene composite. *Polym Degrad Stab* 96(1): 43-50. doi: 10.1016/j.polymdegradstab.2010.11.010
4. Guerrero G, Mutin PH, Vioux A. 2001. Anchoring of phosphonate and phosphinate coupling molecules on Titania particles. *Chem Mater* 13(11): 4367-4373. doi: 10.1021/cm001253u
5. Feng X, Zhai J, Jiang L. 2005. The fabrication and switchable superhydrophobicity of TiO_2 nanorod films. *Angew Chem Int Ed Engl* 44(32): 5115-5118. doi: 10.1002/anie.200501337
6. Bavykin DV, Cressey BA, Light ME, Walsh FC. 2008. An aqueous, alkaline route to titanate nanotubes under atmospheric pressure conditions. *Nanotechnology* 19(27): 275604. doi: 10.1088/0957-4484/19/27/275604
7. Sebastião PJ. 2014. The art of model fitting to experimental. *Eur J Phys* 35: 015017. doi: 10.1088/0143-0807/35/1/015017
8. Khanam R, Mohanta D. 2013. Properties of hydrothermally processed multi-walled titania nanotubes. *Physica E Low Dimens Syst Nanostruct* 49: 39-43. doi: 10.1016/j.physe.2013.01.012
9. Tsai CC, Teng H. 2006. Structural features of nanotubes synthesized from NaOH treatment on TiO_2 with different post-treatments. *Chem Mater* 18(2): 367-373. doi: 10.1021/cm0518527
10. da Silva WL, Lansarin MA, Moro CC. 2013. Synthesis, characterization and photocatalytic activity of nanostructured TiO_2 catalysts doped with metals. *Química Nova* 36(3): 382-386. doi: 10.1590/S0100-40422013000300006
11. Teixeira VG, Coutinho FMB, Gomes AS. 2001. The most important methods for the characterization of porosity of styrene-divinylbenzene based resins. *Química Nova* 24(6): 808-818. 10.1590/S0100-40422001000600019
12. Costa ACFM, Vilar MA, Lira HL, Kiminami RHGA, Gama L.

2006. Synthesis and characterization of TiO_2 nanoparticles. *Cerâmica* 52(324): 255-259. doi: 10.1590/S0366-69132006000400007

13. Sing KSW, Everett DH, Haul RAW, Moscou L, Pierotti RA, et al. 1986. Reporting physisorption data for gas/solid systems — with special reference to the determination of surface area and porosity. *Pure & Appl Chem* 57(4): 603-619.
14. Zhao L, Yu J. 2006. Controlled synthesis of highly dispersed TiO_2 nanoparticles using SBA-15 as hard template. *J Colloid Interface Sci* 304(1): 84-91. doi: 10.1016/j.jcis.2006.08.042
15. Fen LB, Han TK, Nee NM, Ang BC, Johan MR. 2011. Applied surface science physico-chemical properties of titania nanotubes synthesized via hydrothermal and annealing treatment. *Appl Surf Sci* 258(1): 431-435. doi: 10.1016/j.apsusc.2011.08.115
16. Nakayama N, Hayashi T. 2007. Preparation and characterization of poly(L -lactic acid)/TiO_2 nanoparticle nanocomposite films with high transparency and efficient photodegradability. *Polym Degrad Stab* 92(7): 1255-1264. doi: 10.1016/j.polymdegradstab.2007.03.026
17. Rodrigues EJR, Nascimento SAM, Tavares MIB, Merat PP. 2012. On the influence of processing parameters on the molecular dynamics of melt intercalated polycarbonate-clay nanocomposites. *Polímeros Ciência e Tecnologia* 22(5): 436-439. doi: 10.1590/S0104-14282012005000058
18. da Silva MA, Tavares MIB, Nascimento SAM, Rodrigues EJR. 2012. Characterization of polyurethane/organophilic montmorilonite nanocomposites by low field NMR. *Polímeros* 22(5): 481-485. doi: 10.1590/S0104-14282012005000064
19. Soares IL, Chimanowsky JP, Luetkmeyer L, da Silva EO, Souza Dde H, et al. 2015. Evaluation of the influence of modified TiO_2 particles on polypropylene composites. *J Nanosci Nanotechnol* 15(8): 5723-5732. doi: 10.1166/jnn.2015.10041